1-1-2014

Total electron scattering cross sections for pyrimidine and pyrazine as measured using a magnetically confined experimental system

M Fuss
Consejo Superior De Investigaciones Científicas

A Sanz
Consejo Superior De Investigaciones Científicas

Francisco Blanco
Universidad Complutense de Madrid

J C. Oller
CIEMAT

Paulo Limao-Vieira
The Open University, Universidade Nova De Lisboa

See next page for additional authors

Total electron scattering cross sections for pyrimidine and pyrazine as measured using a magnetically confined experimental system

Abstract

In this paper, a recently constructed apparatus for measuring electron scattering cross sections while applying a strong axial magnetic field is utilized for determining total scattering cross sections. The first molecules studied with this setup are pyrimidine (1,3-diazine) and pyrazine (1,4-diazine), whose total cross sections are obtained for the incident electron energy range of 8-500 eV. Quite good agreement with earlier theoretical predictions is found after accounting for the angular acceptance (angular resolution for forward scattering) of the apparatus. However, no other experimental total cross sections for electron scattering from pyrimidine or pyrazine have been found in the literature for comparison.

Keywords

cross, scattering, electron, total, confined, magnetically, measured, system, pyrazine, experimental, pyrimidine, sections

Disciplines

Engineering | Science and Technology Studies

Publication Details

Fuss, M. C., Sanz, A. G., Blanco, F., Oller, J. C., Limao-Vieira, P., Brunger, M. J. & Garcia, G. (2014). Total electron scattering cross sections for pyrimidine and pyrazine as measured using a magnetically confined experimental system. Journal of Physics: Conference Series, 488 1-8.

Authors

M Fuss, A Sanz, Francisco Blanco, J C. Oller, Paulo Limao-Vieira, M J. Brunger, and Gustavo García

Total electron scattering cross sections for pyrimidine and pyrazine as measured using a magnetically confined experimental system

XXVIII International Conference on Photonic, Electronic and Atomic Collisions (ICPEAC 2013) IOP Publishing
Journal of Physics: Conference Series **488** (2014) 012048 doi:10.1088/1742-6596/488/1/012048

Total electron scattering cross sections for pyrimidine and pyrazine as measured using a magnetically confined experimental system

M C Fuss[1], A G Sanz[1], F Blanco[2], J C Oller[3], P Limão-Vieira[4], M J Brunger[5,6] and G. García[1,7]

[1] Instituto de Física Fundamental, Consejo Superior de Investigaciones Científicas, 28006 Madrid, Spain
[2] Departamento de Física Atómica, Molecular y Nuclear, Universidad Complutense de Madrid, 28040 Madrid, Spain
[3] Centro de Investigaciones Energéticas, Medioambientales y Tecnológicas (CIEMAT), 28040 Madrid, Spain
[4] Laboratório de Colisões Atómicas e Moleculares, CEFITEC, Departamento de Física, Faculdade de Ciências e Tecnologia, Universidade Nova de Lisboa, 2829-516 Caparica, Portugal
[5] ARC Centre for Antimatter-Matter Studies, School of Chemical and Physical Sciences, Flinders University, G.P.O. Box 2100, Adelaide, South Australia 5001, Australia
[6] Institute of Mathematical Sciences, University of Malaya, Kuala Lumpur, Malaysia
[7] Centre for Medical Radiation Physics, University of Wollongong, NSW2522, Australia

E-mail: g.garcia@iff.csic.es

Abstract. In this paper, a recently constructed apparatus for measuring electron scattering cross sections while applying a strong axial magnetic field is utilized for determining total scattering cross sections. The first molecules studied with this setup are pyrimidine (1,3-diazine) and pyrazine (1,4-diazine), whose total cross sections are obtained for the incident electron energy range of 8–500 eV. Quite good agreement with earlier theoretical predictions is found after accounting for the angular acceptance (angular resolution for forward scattering) of the apparatus. However, no other experimental total cross sections for electron scattering from pyrimidine or pyrazine have been found in the literature for comparison.

1. Introduction

It is well known [1] that high energy radiation produces abundant secondary electrons ($\sim 4 \cdot 10^4$ per MeV of energy primarily transferred), which are the main source of the energy deposition map and radiation damage in biological tissues. These low-energy, possibly even sub-ionizing, electrons play an important role for inducing damage such as strand breaks or molecular dissociations in biomolecular systems, as has been extensively demonstrated [e.g. 2–4]. Therefore, when studying radiation effects in biological media, it is essential that the particular electron interaction parameters are well known.

In view of this total cross sections (CSs) represent a vital self-consistency check for the accuracy of independently determined integral cross sections, as the total cross section at a given energy is the sum of the integral cross sections for all possible scattering processes. The preliminary total CS measurements we report here have been carried out using a newly

constructed apparatus. This system for measuring electron scattering cross sections is based on the strong axial magnetic confinement of the electrons inside the collision chamber. The technique permits, in principle, the simultaneous measurement of the total scattering CS, integral cross sections for elastic and different inelastic processes (depending on the associated energy loss), and absolute differential CSs [5]. The molecular targets studied here are pyrimidine and pyrazine, whose total scattering CS we have measured for incident energies in the range 8–500 eV and 10–500 eV, respectively.

While pyrimidine forms the molecular basis of several biological molecules, such as cytosine, thymine, uracil, thiamin and alloxan, pyrazine is considered to be its high-symmetry isomer of interest. Both diazines are stable to heating and have their liquid phases at normal pressure closer to room temperature, making them much more accessible model systems for scattering experiments, particularly those in the gaseous phase. Regarding the electron scattering behaviour, their main difference is the permanent dipole moment of 2.28–2.39 D [6–8] for pyrimidine and 0 D for pyrazine. We notice electron scattering calculations to pyrimidine and pyrazine [9–17], as well as some experimental studies [10, 12, 18–25]. However, experimental total CSs have, to the best of our knowledge, so far only been reported for positron scattering from pyrimidine [11, 26].

2. Experimental methods

A recently constructed experimental system for measuring electron scattering cross sections, within a strong axial magnetic field, was used to perform our total scattering cross section measurements. The functionality of this apparatus is based on the magnetic confinement of the electron beam from its entrance into the collision chamber until its detection, so that scattered and unscattered electrons are detected together after their energy analysis. The role of the main magnetic field (0.2 T) is thus simply to translate the electron–which exhibits the exact angle and energy that resulted from a potential collision–along the central axis to the end of the collision chamber. This apparatus has been recently described in some detail [27], therefore only a brief summary is given here.

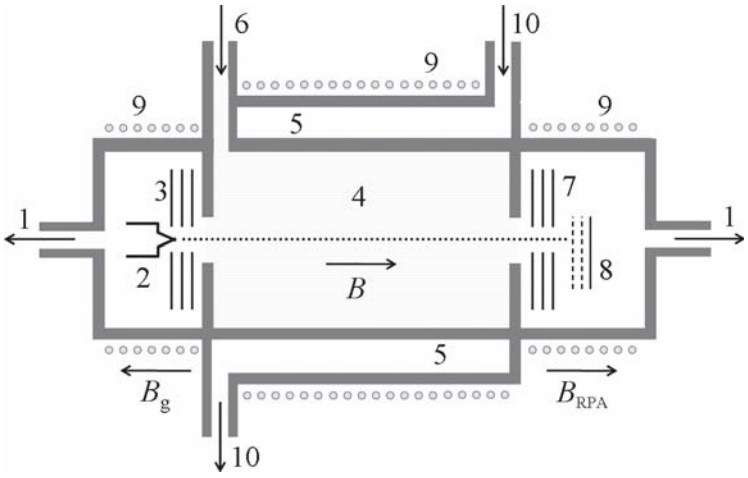

Figure 1. Sketch of the experimental apparatus: 1 - turbomolecular pumps, 2 - electron-emitting filament, 3 - extraction and acceleration electrodes, 4 - collision chamber, 5 - water jacket, 6 - gas inlet, 7 - retarding potential analyzer (RPA), 8 - electron detector (microchannel plate assembly), 9 - magnetic coils, 10 - cooling liquid inlet/outlet.

The whole apparatus (a schematic diagram is given in figure 1) consists of three regions (electron gun, collision chamber and analyzer-detector region), connected by small orifices, which have independent magnetic fields. Electrons are obtained by thermionic emission from a tungsten filament (2) and accelerated to a kinetic energy E before passing into the collision chamber (4). The magnetic field B_{g} of the electron gun region, oriented opposing the main field B, ensures a low angular spread of the electron beam by locally compensating B and preventing electrons leaving the filament in oblique directions to pass the collimators.

The collision chamber itself has a geometrical length of 140 mm and is therefore sufficiently large compared to the delimiting apertures (1 and 2.3 mm) to guarantee a well-defined region of constant pressure. The molecules are introduced into the system via a heated variable leak valve (6), from a steel sample container maintained at around 40°C by means of various silicone heater mats. The chamber wall can partly absorb the heat dissipated by the magnetic coils (9), depending on the pumping speed of the cooling liquid through the chamber's water jacket (5). Hence, the balance between solenoid current and water speed can be utilized in order to maintain a convenient chamber temperature and avoid condensation of the sample on the inner walls. The pressure in the chamber is determined by a Baratron capacitance manometer (MKS, Germany) and the temperature is measured using a K-type thermocouple in thermal contact with the inner chamber wall. Owing to the magnetic confinement, the effective localization of electrons after scattering (before entering the analyzer) is within a radius of 1 mm around the central axis.

After traversing the collision chamber, electrons are selected by a retarding potential analyzer (RPA) so that only electrons with parallel (axial) components of the kinetic energy $\geq eV_R$ (where e represents the elementary charge and V_R is the retarding potential) continue towards the detector. Note that electrons scattered backwards (>90°) are reflected by the electron gun electrostatic lens system and traverse the collision chamber a second time before reaching the analyzer. The detector assembly is formed by two microchannel plates (Hamamatsu photonics, Japan) and an anode and is run at $\sim +2$ keV. It is operated in single-pulse counting mode and connected, via some additional electronics, to a PC running a custom LabView (National Instruments) programme which registers the pulses.

Pyrimidine and pyrazine with a stated purity of 99% were purchased from Sigma-Aldrich and further purified through the performance of freeze-pump-thaw cycles. Before each measurement, the energy resolution $\delta E = e(V_{R,90} - V_{R,10})/2$, with $V_{R,90}$ and $V_{R,10}$ being the retarding potentials leading to 90% and 10% of transmitted electrons, was obtained from the transmission curve $I(V_R)$ in vacuum, where I is the transmitted beam intensity (electron count rate). It was generally found to be similar to the FWHM (full width at half maximum) of the derivative of the transmission curve. Subsequently, the retarding potential (energy cut-off) value was fixed at 85% of the maximum beam intensity in vacuum, i.e. in such a way that the higher-energetic 85% of all electrons were transmitted and included in the total CS measurement. A series of 7–10 attenuation curves, each comprising normally 7–12 data pairs (pressure (p) and intensity (I)), was then acquired. The data points were fitted with an exponential curve $I(p)$ from which the experimental scattering cross section σ_{exp} is obtained according to the Beer-Lambert law,

$$I = I_0 e^{-nl\sigma_{\mathrm{exp}}} = I_0 e^{-pl\sigma_{\mathrm{exp}}/kT}. \tag{1}$$

Here, I_0 is the intensity of the unattenuated beam (in vacuum), n is the number density of the target gas, $l = 141.3$ mm is the effective collision chamber length, k is the Boltzmann constant, and $T = \sqrt{T_{\mathrm{C}} T_{\mathrm{m}}}$ is the gas temperature (K) calculated according to the thermal transpiration effect [28] between the manometer at T_{m} and the collision chamber at T_{C}. For further details on the experimental apparatus and procedures, please refer to reference [27].

2.1. Measurement uncertainties

The experimental uncertainty for the present measurements lies within the range 1.8–5% (for incident energies ≥20 eV and ≤15 eV, respectively). These values include contributions from the uncertainties in the determination of the collision chamber length, sample gas pressure, temperature and incident beam energy. Furthermore, a statistical reproducibility (standard deviation between curves of the same series) of typically ≤3%, comprising filament emission stability, temperature stability, and the uncertainty in the determination of the fit function (exponent of the attenuation curve) has been observed. Combining the aforementioned factors, one obtains a general precision of the present experimental total cross section determination of 3.5–4.4% at incident energies ≥20 eV, and of <5.1% for incident energies ≤15 eV.

In addition to this general uncertainty of statistical nature, the angular acceptance $\delta\theta$ of the apparatus is a limiting aspect and represents an important systematic error source. Due to the axial magnetic confinement, even scattered electrons will pass the RPA if the kinetic energy $E'_{\parallel}$, corresponding to the parallel component of their velocity ($v'_{\parallel}$), can overcome the retarding potential V_R, i.e. $m_e {v'_{\parallel}}^2/2 \geq eV_R$ (where m_e is the electron mass). If this applies, the electron is identified as 'unscattered' and fails to contribute to the measured beam attenuation. The angular resolution in forward direction (angular acceptance of elastically scattered electrons during total cross section measurements) can thus be calculated from the energy resolution δE, obtained from the transmission curve, using:

$$\delta\theta = \arcsin\sqrt{\delta E/E}\,. \tag{2}$$

$\delta\theta$ of the present measurements was between 3.3° and 18.2°. Any comparison to other total cross section data should take into account that, according to the above, the present experimental values σ_{exp} represent in fact apparent values:

$$\sigma_{\mathrm{exp}}(E) \approx \sigma(E) - \sigma_{\mathrm{forw}}(E) \tag{3}$$

with

$$\sigma_{\mathrm{forw}} = 2\pi\Big(\int_0^{\delta\theta} \frac{\mathrm{d}(\sigma_{\mathrm{el}}+\sigma_{\mathrm{rot}})}{\mathrm{d}\Omega}\sin\theta\mathrm{d}\theta + \int_{180-\delta\theta}^{180} \frac{\mathrm{d}(\sigma_{\mathrm{el}}+\sigma_{\mathrm{rot}})}{\mathrm{d}\Omega}\sin\theta\mathrm{d}\theta\Big), \tag{4}$$

where σ_{el} and σ_{rot} denote the integral elastic and rotational CS, respectively.

3. Results

3.1. Pyrimidine

The experimental cross section values $\sigma_{\mathrm{exp}}(E)$ we obtained in the incident energy range 8–500 eV for pyrimidine are presented in figure 2. Note that, due to some minor geometrical misalignment inside the electron gun in the current configuration, the energy and consequently angular resolutions presented a sudden increase in value for three of the higher incident energies—200, 400 and 500 eV—which results in relatively lower total CS values for those energies. For comparison, our IAM-SCAR results [17], a recent scaled quasi-free scattering model (SQFSM) total CS calculation [16], and a low-energy R-matrix calculation [17] are also depicted.

The integral elastic CS reported in reference [12] is not included in the comparison since it, as in most experimental studies on elastic scattering, is actually the result of an extrapolation towards 0° and 180° of the differential cross section measurements conducted within a restricted angular range. As a consequence the integral elastic CS is afflicted with a considerably higher uncertainty than the individual DCS data points from which it was derived.

It can be seen in figure 2 that the experimental values generally exhibit quite good agreement (<5–10% difference) with the IAM-SCAR scattering cross section, when the latter is calculated under the experimental conditions. Note, however, that higher differences (up to 16%) appear

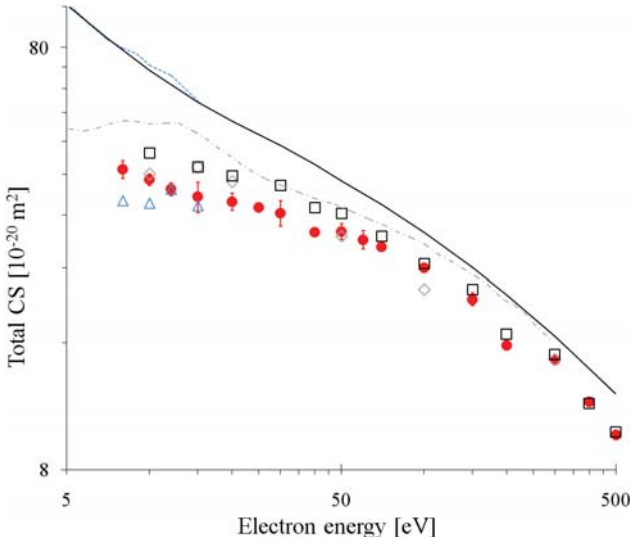

Figure 2. Total CS σ_{exp} measured for electron scattering from pyrimidine (•). Error bars reflect the combined statistical uncertainty of a data point according to section 2.1. ——, IAM-SCAR calculation including dipole-induced rotations [11, 17]; — · —, Born-dipole-corrected SQFSM [16] total CS; - - - -, Born-corrected R-matrix total CS [17]. CSs $\sigma - \sigma_{\mathrm{forw}}$ emulating the experimental conditions are also given for the theoretical IAM-SCAR (□), SQFSM [16] (♢) and R-matrix [17] (△) results in order to facilitate comparison.

in the energy range 8–40 eV, where the experimental values lie below theory. Nonetheless both sets of results agree to within the combined uncertainty limits. When comparing the present experiment to the SQFSM results for $\sigma - \sigma_{\mathrm{forw}}$, as derived from reference [16], a similar overall level of agreement is observed. The differences in the total CSs, in the overlapping energy range, with the R-matrix CS for $\sigma - \sigma_{\mathrm{forw}}$, as derived from reference [17], fall also within a very similar magnitude (0.1–17%). However in this case the theoretical prediction consistently underestimates the measured CS. These discrepancies between the present measured total CS and the different calculations (especially with regard to IAM-SCAR and R-matrix, which closely agree in the total CS σ), when comparing $\sigma - \sigma_{\mathrm{forw}}$, clearly indicate the importance of the elastic angular distribution when attempting to compare experimental and calculated total CS values (while accounting for the known experimental angular resolution). Nonetheless, the differences found in all our comparisons are still quite reasonable, taking into account that the calculated dipole- or Born-corrected elastic DCS all present large gradients in the forward direction that strongly influence the result of the partial integration. Additionally, the theoretical absorption (inelastic) CSs from references [16] and [11] only start to rise in magnitude for the lower energies studied here and might thus be affected by a higher uncertainty in the sense of an underestimation of their true value. At the same time, the R-matrix approach does not account for ionization and so aims to provide an accurate total CS only up to about 10 eV. Summarizing, a pleasing overall level of agreement between the present experimental total CS and previous theoretical studies [12, 16, 17] is obtained, especially after noting that the experimental data largely lie between the different theoretical results.

3.2. Pyrazine

The experimental cross sections $\sigma_{\mathrm{exp}}(E)$ that were obtained for the incident energies 10–500 eV in pyrazine are presented in figure 3, together with our IAM-SCAR total CS values and a low-energy R-matrix total CS [13]. Note that as before, some minor geometrical misalignment in the electron gun causes the energy and consequently angular resolutions to suffer from relatively increased values at the high incident energies. In order to account for the angular acceptance $\delta\theta$ of the apparatus observed during each measurement, again $\sigma - \sigma_{\mathrm{forw}}$ was calculated using alternatively the IAM-SCAR and R-matrix values. As before, this is included to facilitate a direct comparison under very similar conditions. Available experimental elastic CS data [20],

integrated using extrapolations towards 0° and 180°, are not shown for comparison for the reasons outlined in the previous section.

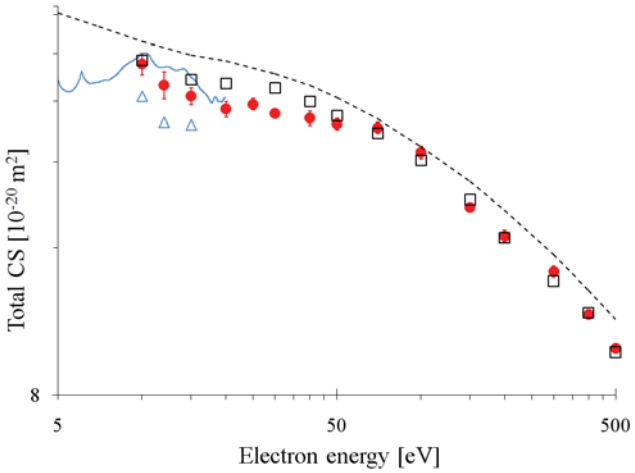

Figure 3. Total CS $\sigma_{\rm exp}$ measured for electron scattering from pyrazine (•). Error bars reflect the combined statistical uncertainty of a datum point, however in some cases they fall within the size of the symbols used. - - - -, IAM-SCAR calculation; ——, R-matrix total CS [13]. CS values $\sigma - \sigma_{\rm forw}$, emulating the experimental conditions, are also given for the theoretical IAM-SCAR (□) and R-matrix (△) results in addition to the original calculated values.

It can be seen in figure 3 that the experimental values are in quite good agreement (to within the uncertainty limits) with the IAM-SCAR values for $\sigma - \sigma_{\rm forw}$ in the whole energy range where the measurements were performed. A maximum difference of 12% (theory higher than experiment) is observed at 20 and 30 eV, while for all other energies, differences are $\leq 8\%$. The comparison of our experimental total CS to the R-matrix cross section for $\sigma - \sigma_{\rm forw}$, in the low energy region, yields differences up to 18%, with the experiment giving larger values in this case. This observation is consistent with the difference in magnitude of the original (full) IAM-SCAR and R-matrix results, yet the different angular distributions predicted by both theories do noticeably influence the values of $\sigma - \sigma_{\rm forw}$ calculated according to emulate the experimental conditions. Particularly in the forward direction, the R-matrix DCSs [13], which give better agreement with the experimental DCSs [20], are much higher in magnitude than the IAM-SCAR DCSs and this explains the larger effect regarding a partial integration of the R-matrix theory elastic DCSs. While in the low energy region the experimental total CS lies between the cross sections $\sigma - \sigma_{\rm forw}$ from the R-matrix and IAM-SCAR methods, with increasing energy, the agreement between the experimental TCS and the IAM-SCAR $\sigma - \sigma_{\rm forw}$ values improves gradually, leading to an excellent level of accord for incident energies $\geq$70 eV.

In figure 4 we present a direct comparison of the experimental total CS obtained for pyrimidine and pyrazine. Note that the total CSs for the two diazines agree very well to within the experimental uncertainty. Both total CSs display a similar energy dependence and only for energies 12 eV $\leq E \leq$ 30 eV does a tendency to diverge become apparent. At first glance, this observation is a little counter-intuitive, as while both species have similar dipole polarizabilities they have very different permanent dipole moments which we might have anticipated would influence the scattering dynamics differently in each case. In contrast, when looking at the theoretical TCS data (figures 2 and 3), important differences are found between pyrimidine and pyrazine, in particular at low energies, due to the strong polar nature of the first molecule and the corresponding dipole-induced rotational excitations especially in the forward angular range. The fact that these differences are not present to a similar intensity in the present experimental results, simply derives from the angular acceptance of the apparatus which is able to discern only a part of the forward-scattered electrons after rotational excitation events.

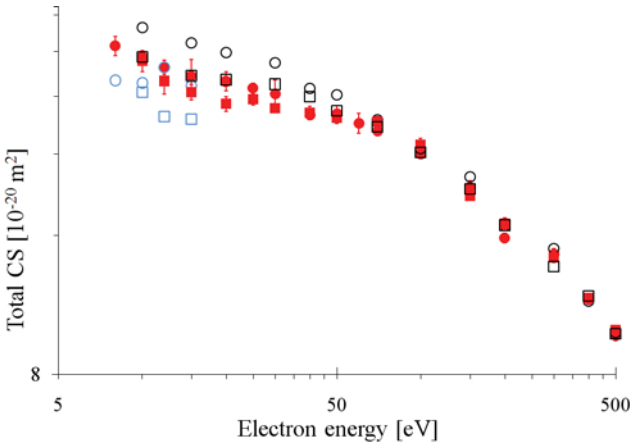

Figure 4. Comparison of total CS results for pyrimidine (●) and pyrazine (■). CSs $\sigma - \sigma_{\text{forw}}$ which emulate the experimental conditions are included for the theoretical IAM-SCAR [11, 17] and R-matrix [13, 17] results: ○, IAM-SCAR pyrimidine; □, IAM-SCAR pyrazine; ○, R-matrix pyrimidine; □, R-matrix pyrazine.

4. Conclusions

Operation of a new experimental apparatus, making use of a strong axial magnetic field for studying electron scattering, has been started with pyrimidine and pyrazine as the first target species. Further to the agreement between the measured cross sections and comparisons with previous theoretical data, we conclude that the present system yields reliable total CSs values. This is particularly true when we allow for the experimental angular acceptance, which determines the angular limit for distinguishing scattered electrons, of the apparatus' configuration. In this context, the IAM-SCAR formalism was shown to be an extremely helpful complement to the experiment for providing partially integrated CS, $\sigma - \sigma_{\text{forw}}$, emulating the experimental conditions, so that a realistic comparison could be achieved. Certainly, the current measurements represent one step further towards the availability of a self-consistent pyrimidine and pyrazine database for simulation [29] or other purposes. However, although the apparatus in its present form shows utility for total CS measurements, we aim to develop it further to achieve better energy (and thus angular) resolution (or near constant resolution of approximately the lowest values obtained here, 0.4 eV) before performing integral elastic and inelastic or differential CS measurements. A better resolution would, additionally, permit more accurate measurements of molecules presenting a large dipole moment and would facilitate an extension of the present energy range up to $\sim$ 1 keV. Our preference for future studies lies on investigating molecules such as uracil and the DNA bases.

Acknowledgments

This study was partially supported by the Ministerio de Ciencia e Innovación (FIS2009-10245 and FIS2012-31320) and the EU Framework Programme (COST Action MP1002). Technical support from the Spanish National Institute for Fusion Research of CIEMAT is acknowledged. MJB thanks the Australian Research Council for some financial support. MCF acknowledges a PIF grant of the Comunidad Autónoma de Madrid. PLV acknowledges FCT-MEC support through PEst-OE/FIS/UI0068/2011 and PTDC/FIS-ATO/1832/2012 grants.

References

[1] Plante I and Cucinotta F A 2009 *New J. Phys.* **11** 063047
[2] Boudaïffa B, Cloutier P, Hunting D, Huels M A and Sanche L 2000 *Science* **287** 1658–1660
[3] Boudaïffa B, Cloutier P, Hunting D, Huels M A and Sanche L 2002 *Radiat. Res.* **157** 227

[4] Huels M A, Boudaïffa B, Cloutier P, Hunting D and Sanche L 2003 *J. Am. Chem. Soc.* **125** 4467–4477

[5] Sullivan J P, Gilbert S J, Marler J P, Greaves R G, Buckman S J and Surko C M 2002 *Phys. Rev. A* **66** 042708

[6] Blackman G L, Brown R D, and Burden F R 1970 *J. Mol. Spectrosc.* **35** 444–454

[7] Kisiel Z, Pszczolkowski L, Lopez J C, Alonso J L, Maris A and Caminati W 1999 *J. Mol. Spectrosc.* **195** 332–339

[8] Chen P Y and Holroyd R A 1996 *J. Chem. Phys.* **100** 4491–4495

[9] Winstead C and McKoy V 2007 *Phys. Rev. A* **76** 012712

[10] Maljković J B, Milosavljević A R, Blanco F, Šević D, García G and Marinković B 2009 *Phys. Rev. A* **79** 052706

[11] Zecca A, Chiari L, García G, Blanco F, Trainotti E and Brunger M J 2010 *J. Phys. B* **43** 215204

[12] Palihawadana P, Sullivan J, Brunger M J, Winstead C, McKoy V, García G, Blanco F and Buckman S J 2011 *Phys. Rev. A* **84** 062702

[13] Mašin Z and Gorfinkiel J D 2011 *J. Chem. Phys.* **135** 144308

[14] Mašin Z and Gorfinkiel J D 2012 *J. Chem. Phys.* **137** 204312

[15] Mašin Z, Gorfinkiel J D, Jones D B, Bellm S M and Brunger M J 2012 *J. Chem. Phys.* **136** 144310

[16] Ferraz J R, dos Santos A S, de Souza G L C, Zanaleto A I, Alves T R M, Lee M T, Brescansin L M, Lucchese R R and Machado L E 2013 *Phys. Rev. A* **87** 032717

[17] Sanz A G, Fuss M C, Blanco F, Mašín Z, Gorfinkiel J D, Carelli F, Sebastinelli F, Gianturco F and García G 2013 *Appl. Radiat. Isotop.* **accepted for publication** http://dx.doi.org/10.1016/j.apradiso.2013.01.031

[18] Levesque P L, Michaud M and Sanche L 2005 *J. Chem. Phys.* **122** 094701

[19] Ferreira da Silva F, Almeida D, Martins G, Milosavljević A R, Marinković B P, Hoffmann S V, Mason N J, Nunes Y, García G and Limão-Vieira P 2010 *Phys. Chem. Chem. Phys.* **12** 6717–6731

[20] Palihawadana P, Sullivan J, Buckman S J and Brunger M J 2012 *J. Chem. Phys.* **137** 204307

[21] Jones D B, Bellm S M, Limão-Vieira P and Brunger M J 2012 *Chem. Phys. Lett.* **535** 30–34

[22] Jones D B, Bellm S M, Blanco F, Fuss M C, García G, Limão-Vieira P and Brunger M J 2012 *J. Chem. Phys.* **137** 074304

[23] Linert I, Dampc M, Mielewska B and Zubek M 2012 *Eur. Phys. J. D* **66** 20

[24] Hein J D, Al-Khazraji H, Tiessen C J, Lukic D, Trocchi J A and McConkey J W 2013 *J. Phys. B* **46** 045202

[25] Colmenares R, Sanz A G, Fuss M C, Blanco F and García G 2013 *Appl. Radiat. Isotop.* **accepted for publication** http://dx.doi.org/10.1016/j.apradiso.2013.01.025

[26] Palihawadana P, Boadle R, Chiari L, Anderson E K, Machacek J R, Brunger M J, Buckman S J and Sullivan J 2013 *Phys. Rev. A* **accepted for publication**

[27] Fuss M, Sanz A G, Blanco F, Oller J C, Limão-Vieira P, Brunger M J and García G 2013 *Phys. Rev. A* **submitted for publication**

[28] Knudsen M 1910 *Ann. Physik* **336** 205

[29] Fuss M C, Sanz A G, Muñoz A, Blanco F, Brunger M J, Buckman S J, Limão-Vieira P and García G 2013 *Appl. Radiat. Isotop.* **accepted for publication** http://dx.doi.org/10.1016/j.apradiso.2013.01.017i